Journal of ELECTRONIC MATERIALS, Vol. 48, No. 6, 2019
https://doi.org/10.1007/s11664-019-07119-4


# Anatase $TiO_2$ Nanotubes-Aggregated Porous Microspheres for Ti Foil-Based Quasi-Solid State Dye-Sensitized Solar Cells with Improved Photovoltaic Performance

JIN HYOK RI,[1,2] GWON IL RYU,[1] SONG GUK KO,[1] BYOL KIM,[1] and KYONG SU SONU[1]

1.—Department of Biophysics, Faculty of Life Science, Kim Il Sung University, Ryongnam-Dong, Taesong District, Pyongyang, Democratic People's Republic of Korea. 2.—e-mail: life3@ryongnamsan.edu.kp

Fibrous anatase $TiO_2$ nanotubes-aggregated porous microspheres (AMS) with high specific surface area (160 $m^2 g^{-1}$) were fabricated through an alkali solution-assisted hydrothermal process followed by an acid post-treatment and a calcination by using commercial $TiO_2$ nanopowder (P25) as raw material. The resultant AMS microspheres with an average diameter of $\sim 5$ $\mu$m have three-dimensional network-like porous structures formed by accumulation and winding of fibrous $TiO_2$ nanotubes with diameter $< 10$ nm. When used as photoanode materials of Ti foil-based quasi-solid state dye-sensitized solar cells, the AMS film-based solar cell gives a conversion efficiency of 7.16% with 34% improvement when compared to the P25 film-based one (5.34%).

**Key words:** Ti foil-based dye-sensitized solar cell, anatase $TiO_2$ microsphere, hydrothermal process, electron transfer, electron lifetime

## INTRODUCTION

Dye-sensitized solar cells (DSSCs) have attracted great interest in academic research and industrial applications as an alternative to the traditional silicon-based devices because of their low-cost and relatively high photovoltaic property.[1–5] In order to improve the power conversion efficiency, many researchers have focused on the development of various nanostructured and/or hierarchical materials for the composition and structure optimization of the photoanodes.[6–11] Thereinto, $TiO_2$ hierarchical structure can effectively improve the light scattering ability, the dye-loading amount and even the electron transport property of DSSCs.[12,13] Among various preparation methods of $TiO_2$ hierarchical structures, the hydrothermal method is the most widely used and effective one, and $TiO_2$ materials or films with different morphologies, crystal phases and micro/nano-structures have been fabricated by changing the hydrothermal reaction conditions.[6,7,13–16]

Up till now, various $TiO_2$ micro/nano-structured materials (such as tubes, rods, bands and their aggregated microspheres or flowers) have been fabricated and used as photoanode materials of DSSCs.[8,17–26] Among which, $TiO_2$ nanotubes have attracted much attention due to its one-dimensional structure, its reduced grain boundaries could improve electron transport and prolong electron lifetimes compared with the conventional $TiO_2$ nanoparticle film photoanode.[20–27] However, most of the single $TiO_2$ nanotubes film-based DSSCs showed unsatisfactory conversion efficiency compared with the $TiO_2$ nanoparticles film-based ones because those nanotubes with diameters $\geq 100$ nm have small specific surface area, which usually leads to insufficient dye-loading.[23,25] For example, it was reported that the commercial $TiO_2$ nanoparticles (P25) film has more than seven times active surface area of $TiO_2$ nanotubes film with the same thickness.[25] In 2012, a self-assembled film of $TiO_2$ nanotubes with high specific surface area (100 $m^2 g^{-1}$) and ultra-fine diameter ($< 10$ nm) was

(Received August 26, 2018; accepted March 7, 2019; published online March 15, 2019)

fabricated and applied to DSSCs on flexible Ti foil.[27] Due to the higher surface area and one-dimensional ultra-fine nanotube structure, 6.23% conversion efficiency was obtained with this self-assembled $TiO_2$ nanotube film, which was superior to that of conventional $TiO_2$ nanoparticles.[27] This result suggested effective tactics for improving the photovoltaic performance of $TiO_2$ nanotubes film-based DSSCs by simultaneously reducing the diameter and maintaining the one-dimensional structure of the nanotubes.

Also, sea urchin-like $TiO_2$ hierarchical microspheres with a specific surface area of 97 $m^2\ g^{-1}$ was prepared and applied to quasi-solid state DSSCs on flexible plastic substrate in Peng's group,[28] and 4.32% conversion efficiency was obtained with this sea urchin-like microspheres film, which was better than that of the P25 film-based one.[28] The hierarchical structure and high surface area of the sea urchin-like microspheres cannot only provide sufficient dye-loading, but also the larger pore size of the film, which is beneficial to the penetration of gel electrolytes in the film. Especially, the hierarchical microspheres containing one-dimensional $TiO_2$ nanostructures can effectively enhance the light scattering and dye-loading, reduce charge recombination and improve electron transport in $TiO_2$ films, thereby improving the conversion efficiency of DSSCs.[27–29]

Herein, fibrous anatase $TiO_2$ nanotubes-aggregated porous microspheres (AMS) with higher specific surface area (160 $m^2\ g^{-1}$) were fabricated through an alkali solution-assisted hydrothermal process followed by an acid post-treatment and a calcination by using commercial $TiO_2$ nanopowder (P25) as raw material. The resultant AMS microspheres with an average diameter of $\sim 5\ \mu m$ have three-dimensional network-like porous structures formed by the accumulation and winding of fibrous $TiO_2$ nanotubes with diameter $< 10$ nm. When used as photoanode materials of Ti foil-based DSSCs, the present AMS microspheres/Ti electrode can not only reduce the electron recombination, but also supply a larger surface area for dye-loading. Furthermore, the fibrous anatase $TiO_2$ nanotubes-aggregated porous microspheres provide sufficient interspaces for the penetration of the iodine-free ionic liquid gel electrolyte with high viscosity,[30] which is necessary for the sufficient electrical contact between $TiO_2$ film and gel electrolyte.[30] The corresponding Ti foil-based quasi-solid state DSSCs assembled by the AMS film electrode gives a conversion efficiency of 7.16%, indicating an improvement of 34% compared to the P25 film-based DSSCs (5.34%) as a direct consequence of the significantly enhanced surface area and dye-loading amount as well as the accelerated electron transport capacity.

## EXPERIMENTAL DETAILS

Fibrous anatase $TiO_2$ nanotubes-aggregated porous microspheres (AMS) were fabricated via an alkali solution-assisted hydrothermal process followed by an acid post-treatment and a calcination by using P25 nanoparticles (Degussa, Germany) as raw material. Typically, 8.0 mL of $H_2O_2$ solution (AR, 30%) was added into 60 mL of NaOH solution (10.0 M) under magnetic stirring, and then 0.50 g of P25 nanoparticles were added into the solution. After stirring for 30 min, the resultant mixture was transferred into a 100 mL Teflon-lined stainless steel autoclave, and then kept at 160°C for 2 h. The resulting material was washed three times with deionized water and absolute ethanol to obtain the precursor, which was added in HCl solution (0.2 M) to replace $Na^+$ with $H^+$. After centrifugation, the mixture was washed with deionized water and absolute ethanol, dried in vacuum for 8 h, and then calcined at 500°C for 3 h with heating rate of 2°C $min^{-1}$ to obtain AMS microspheres.

Ti foil-based $TiO_2$ film electrode was prepared through a doctor blading technique according to previous reports.[6,7] The Ti foil substrate (0.1 mm thickness, Wuhan Geao) was cut into $2 \times 3\ cm^2$ sheets, and pre-treated by $HNO_3$/HF mixed solution for 5 min and ultrasonically cleaned in detergent water, acetone, and ethanol before use. Typically, AMS microspheres paste was prepared as follows: a 1.0 g portion of the AMS powder, 0.2 mL of acetic acid, 3.2 mL of terpineol and 0.5 g of ethylcellulose were added in 5.0 mL of ethanol and stirred for 10 h. The resultant paste was scraped onto the pre-treated Ti foil with adhesive tape (Scotch, $\sim 50\ \mu m$) serving as spacer. The obtained film electrode was dried in air and then calcined at 500°C for 30 min. For comparison, P25 film-based photoanode was also prepared by using P25 nanoparticles instead of AMS microspheres.

To improve the electrical contacts among the $TiO_2$ micro/nano-structured films, those obtained Ti foil-based $TiO_2$ film electrodes were post-treated with 1.0 wt.% $TiCl_4$ solution at 70°C for 1 h and then calcined at 500°C for 30 min. Dye-sensitized film electrode was prepared by immersing the resultant $TiO_2$ film electrode into an ethanol solution (0.3 mM) of *cis*-bis(isothio-cyanato)bis(2,2′-bipyridyl-4,4′-dicarboxylato)ruthenium(II) bis(tetrabutylammonium) (N719, Solaronix SA, Switzerland) for 20 h, and then washed with anhydrous alcohol and dried by blow drying.

Since the optical opacity of Ti foil requires the incident light illuminating from the counter electrode of DSSCs (the back-side illumination), the light absorption of the traditional $I_3^-/I^-$ organic electrolyte retards the improvement of the solar cell's photovoltaic performance. Therefore, a

transparent Pt counter electrode was prepared by dropping and spreading $H_2PtCl_6$ isopropanol solution (3.0 mM) on FTO glass followed by heating at 400°C for 30 min. Also, an iodine-free ionic liquid (IL) gel electrolyte was prepared according to a previous report.[30] This iodine-free IL gel electrolyte has much better transparency than the traditional organic electrolytes, and, thus, is beneficial for the Ti foil-based solar cell that needs the back-side illumination.

The iodine-free IL gel electrolyte was cast on the top of a dye-sensitized $TiO_2$ film photoanode, and the transparent Pt counter electrode was assembled to finish the typical sandwich typed Ti foil-based solar cell. A light-shading mask was used on the solar cell to fix the active area to 0.16 $cm^2$.

X-ray powder diffraction (XRD) pattern was obtained by a Miniflex 600 x-ray diffractometer with CuK$\alpha$ irradiation ($\lambda$ = 0.15418 nm) at 40 kV and 15 mA. A scan rate was 4° $min^{-1}$ in the range of $20° \le 2\theta \le 50°$. The morphologies of the $TiO_2$ films on Ti foils were observed by using a field emission scanning electron microscope (FESEM, Zeiss-Sigma). The high-resolution transmission electron microscopy (HRTEM) observation was observed by using a LaB6 JEM-2100(HR) electron microscope (JEOL Ltd.) working at 200 kV. Liquid $N_2$ adsorption–desorption isotherms at 77 K were measured by a Micrometrics ASAP 2010 system.

The thicknesses of Ti foil-based $TiO_2$ films were measured by using a TalyFormvS4C-3D profilometer (U.K.). To estimate the dye-loaded amount on the $TiO_2$ films, the dye-sensitized electrode was immersed into a NaOH solution (0.1 M) in a mixed solvent (water:ethanol = 1:1) at room temperature, which leads to the N719 desorption from film electrode. The absorbance of the resulting solution was determined by a UV-3600 UV–vis spectrophotometer (Shimadzu, Japan). The dye-loaded amount was calculated by the molar extinction coefficient of $1.41 \times 10^4$ $dm^3$ $mol^{-1}$ $cm^{-1}$ at 515 nm as in the previous reports.[6,7,18]

The fabricated solar cell was illuminated by light with energy of a 100 mW $cm^{-2}$ from 300 W simulated sunlight (AM1.5G, 2 × 2 beam, w/6258 lamp, Newport, USA). A SRC-1000-TC-QZ-N monocrystalline silicon cell system (Oriel, USA) that was calibrated by National Renewable Energy Laboratory, A2LA accreditation certificate 2236.01 was used to determine the incident light intensity, and a CHI618 electrochemical analyzer (CH Instruments) was used to collect the current–voltage ($J$–$V$) curves of the solar cells.

The electrochemical impedance spectra (EIS) of those fabricated solar cells were measured with applying bias of the open-circuit voltage ($V_{oc}$) and a frequency range from 0.05 Hz to $10^5$ Hz with AC amplitude of 10 mV. The photoinduced open-circuit voltage decay (OCVD) curves were recorded after the illumination of the solar cell (illuminated to a steady voltage) was turned off by using a shutter. Both of the EIS and OVCD curve measurements were carried out on a CHI604C electrochemical analyzer (CH Instruments) combined with a Xe-lamp as the light source under ambient conditions.

## RESULTS AND DISCUSSION

Figure 1 shows the x-ray powder diffraction (XRD) patterns of the obtained AMS microspheres and P25. It can be seen that all the diffraction peaks of the AMS microspheres at $2\theta$ = 25.3°, 37.9° and 48.3° belong to (101), (004) and (200) planes of anatase $TiO_2$ (JCPDS No. 21-1272),[27] respectively. No diffraction peaks indexed to the rutile phase are detected, indicating that the rutile phase in P25 (Fig. 1) was completely transformed into anatase during the hydrothermal reaction and post-treatment processes. Moreover, no diffraction peak indexed to sodium titanate can be observed in the XRD pattern, implying the $Na^+$ ions have been completely replaced with $H^+$ ions during the post-treatment processes.[27] In addition, the AMS microspheres exhibit much lower crystallinity than the initial P25, which might relate to the changes of crystal phase and microstructure due to the chemical reaction of P25 during the hydrothermal reaction and the post-treatment processes.

FESEM and TEM images shown in Fig. 2 indicate that obtained AMS product has microsphere-like morphology with an average diameter of ~ 5 $\mu$m (Fig. 2a and b), which is composed of long fibrous nanostructures with hundreds of nanometers (Fig. 2c). TEM image (Fig. 2d) shows that the AMS microspheres have a three-dimensional network-like porous structure formed by accumulation and winding of fibrous nanostructures, which are anatase $TiO_2$ nanotubes with a diameter of < 10 nm (Fig. 2e). From the HRTEM image (Fig. 2f), it can be observed that the diameter and wall thickness of those fibrous $TiO_2$ nanotubes are ~ 7 nm and ~ 2 nm, respectively. This unique fibrous anatase $TiO_2$ nanotubes-aggregated porous micro/nanostructures of the obtained AMS microspheres should have larger surface area and a better dye-loading capacity as photoanode material.

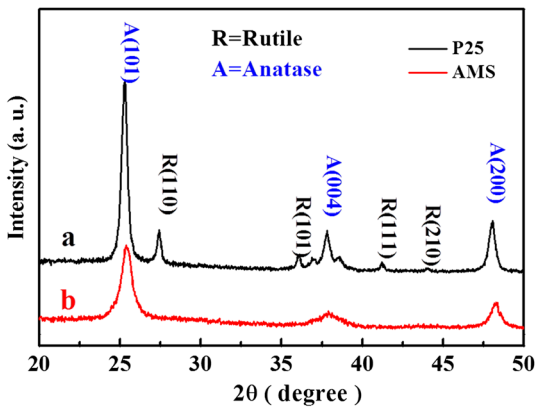


Fig. 1. Typical XRD patterns of the obtained AMS microspheres and P25 nanoparticles.

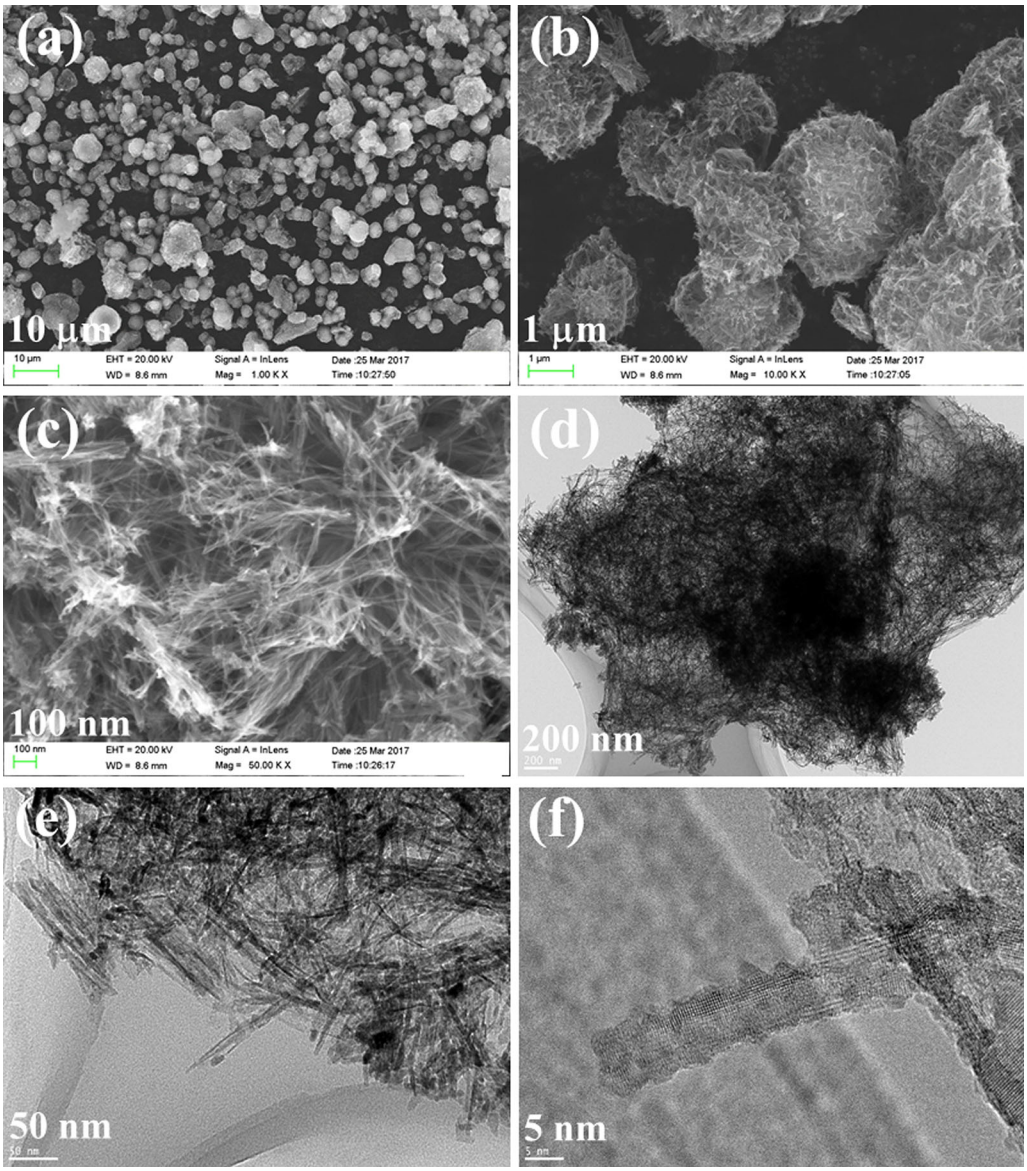


Fig. 2. FESEM (a–c), TEM (d, e) and HRTEM (f) images of the obtained AMS microspheres.

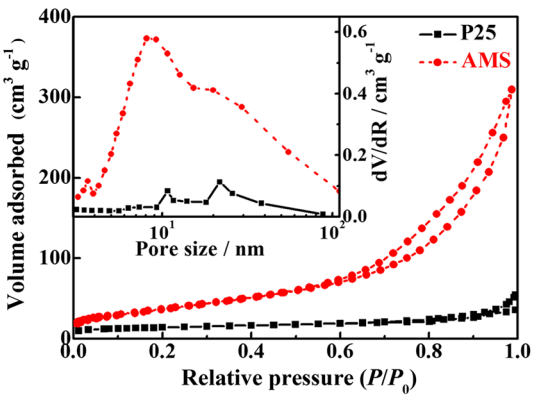


Fig. 3. $N_2$ adsorptione-desorption isotherms and its BJH pore size distribution plots (inset) of AMS microspheres and P25 nanoparticles.

Figure 3 shows the liquid $N_2$ adsorption–desorption isotherms and the Barret–Joyner–Halenda (BJH) pore size distribution plots (inset) of AMS microspheres and P25 nanoparticles. As can be seen, the AMS microspheres exhibit a typical type IV isotherm, which is usually attributed to the predominance of mesopores.[27] The corresponding Brunauer–Emmett–Teller (BET) specific surface area ($S_{BET}$) of the AMS microspheres is $\sim 160$ $m^2$ $g^{-1}$, about 3.6 times as much as that ($\sim 45$ $m^2$ $g^{-1}$) of the P25 nanoparticles. Also, the present AMS microspheres have much larger $S_{BET}$ than previously reported ultra-fine $TiO_2$ nanotubes self-assembled film (100 $m^2$ $g^{-1}$)[27] and sea urchin-like $TiO_2$ hierarchical microspheres (97 $m^2$ $g^{-1}$).[28] The inserted BJH pore size distribution plots show that the obtained AMS microspheres contain three types of pores.

The first type may be ascribed to a smaller portion of mesopores (centered at ~ 3.6 nm) attributed to the nanotubes, the second type (centered at ~ 8.6 nm) and the third type (shoulder peak at ~ 20 nm) could be due to the accumulation and winding of fibrous nanotubes; whereas P25 only shows much smaller pore size distribution peaks centered at 10.8 nm and ~ 22 nm, respectively. Moreover, the present AMS microspheres exhibit a much larger total pore volume (~ 0.48 $cm^3$ $g^{-1}$) than that (~ 0.08 $cm^3$ $g^{-1}$) of P25 nanoparticles. These much broader pore size distribution and larger pore volume of the AMS microspheres can be mainly due to the contribution of those voids formed by accumulation and winding of $TiO_2$ nanotubes within the microspheres, which would be a benefit to the dye loading and the penetration of gel electrolyte when it was used as photoanode material.

The above characterization results indicate that P25 nanoparticles can be transformed into three-dimensional network-like hierarchical microspheres with porous structure and fibrous anatase $TiO_2$ nanotubes under the present preparation processes. Figure 4 shows the formation process of $TiO_2$ anatase nanotube aggregated microstructure through the device schematic. According to the literature,[27] the possible transformation processes can be described as follows. P25 nanoparticles react with NaOH solution in the hydrothermal environment and are transformed into sodium titanate sheets, which then peel off and curl into fibrous nanotube-like structures. By adding into HCl solution, those sodium titanate nanotubes are transformed into titanic acid nanotubes due to the $Na^+$ ions replaced by $H^+$ ones, and then transformed to anatase $TiO_2$ nanotubes by heat treatment at 500°C.[27] The present AMS microspheres have three-dimensional network-like porous microstructure formed by the accumulation and winding of fibrous anatase $TiO_2$ nanotubes with diameter < 10 nm. This small sized fibrous $TiO_2$ nanotubes in the microsphere film electrode can play important roles for increasing the dye-loading amount and providing a direct electron transportation path,[27] and the larger pore volume could promote the penetration of the used gel electrolyte. Both of them are beneficial for improving the photovoltaic performance of DSSCs. Figure 5 shows the current–voltage ($J$–$V$) curves of the Ti foil-based quasi-solid state solar cells fabricated with AMS microspheres and P25 nanoparticles film electrodes under AM 1.5G (1 sun) light illumination. The corresponding photovoltaic performance parameters are listed in Table I. As shown in Table I, the Ti foil-based solar cell using P25 nanoparticles performs a 5.34% conversion efficiency ($\eta$) with an open-circuit voltage ($V_{oc}$) of 0.67 V, a short-circuit current density ($J_{sc}$) of 12.35 mA $cm^{-2}$, and a fill factor (FF) of 0.65. By using the AMS microspheres film, the corresponding device gives a significantly enhanced $J_{sc}$ value (16.63 mA $cm^{-2}$), which mainly contributes the much better efficiency (7.16%) since the $V_{oc}$ and FF values are very similar to those of the P25 film-based device. This result indicates that the present AMS microspheres are superior to the conventional P25 nanoparticles in the application of Ti foil-based DSSCs.

The remarkably enhanced $J_{sc}$ value of the AMS film-based device can be due to the unique micro/-nano-structures of the AMS microspheres with much larger specific surface area and pore volume than the P25 nanoparticles (Fig. 3), which causes the dye-loading amount ($9.8 \times 10^{-7}$ mol $cm^{-2}$) of the AMS film to be about 1.85 times as much as that ($5.3 \times 10^{-7}$ mol $cm^{-2}$) of the P25 film (Table I). More dye molecules in the AMS film are a benefit for more effective light harvesting, which can lead to more photogenerated electrons, and thus to the significantly enhanced $J_{sc}$ value compared to the P25 film-based device. Nevertheless, the above structure and crystal phase analyses indicate that the crystallinity and the primary particle size of the fibrous anatase $TiO_2$ nanotubes in the AMS microspheres are much lower and smaller than those of P25 nanoparticles (Figs. 1 and 2). These features

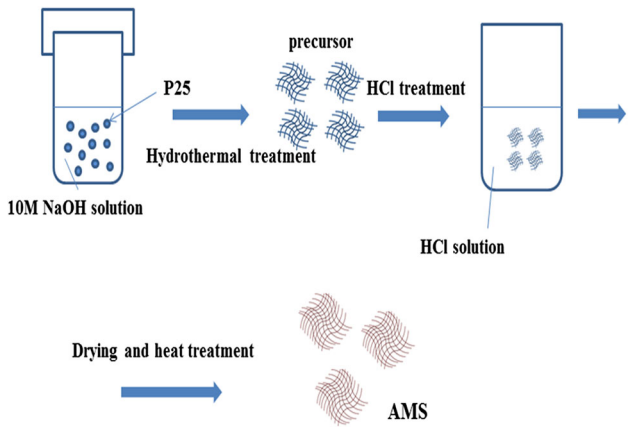


Fig. 4. Schematic illustration of the preparation process of AMS via two steps of reactions.

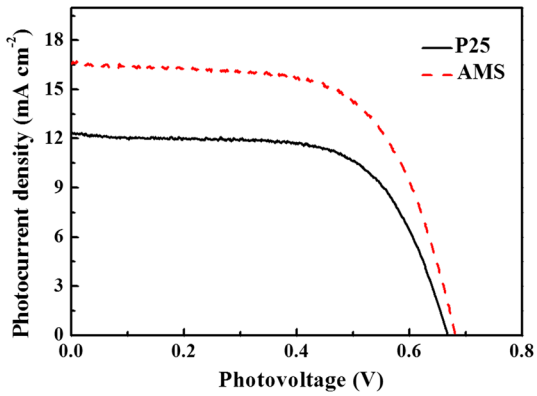


Fig. 5. $J$–$V$ curves of the Ti foil-based quasi-solid state DSSCs fabricated with AMS or P25 film-based electrode.

**Table I. Photovoltaic performance parameters of the Ti foil-based quasi-solid state DSSCs fabricated with AMS or P25 film**

| Device | $J_{SC}$ (mA cm$^{-2}$) | $V_{OC}$ (V) | FF | PCE (%) | Dye loading ($\times 10^{-7}$ mol cm$^{-2}$) |
|---|---|---|---|---|---|
| P25 | 12.35 ± 0.51 | 0.67 ± 0.01 | 0.65 ± 0.03 | 5.34 ± 0.23 | 5.3 ± 0.3 |
| AMS | 16.63 ± 0.64 | 0.68 ± 0.02 | 0.63 ± 0.02 | 7.16 ± 0.36 | 9.8 ± 0.5 |

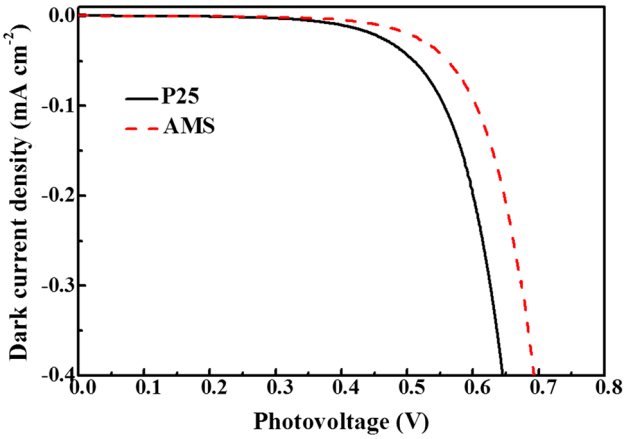


Fig. 6. Dark current curves of the Ti foil-based quasi-solid state DSSCs fabricated with AMS or P25 film-based electrode.

usually cause more charge recombination sites, and then an increased dark current of DSSCs,[27,28] but the AMS film-based solar cell shows less dark current values than the P25 film-based one as can be seen from Fig. 6. It implies that the current leakage can be suppressed when the AMS microspheres were used to replace the P25 nanoparticles.

One possible reason for this issue might be ascribed to the long fibrous anatase $TiO_2$ nanotubes accumulated and wound in the AMS microspheres, which would provide a good path for the electron transport, and thus effectively reduce the charge recombination within the porous film electrode. In addition, the fibrous nanotubes-aggregated AMS microspheres with three-dimensional network-like porous structure can provide sufficient interspaces for the penetration of the IL gel electrolyte with high viscosity,[30] thereby improving the electron transfer rate between the electrolyte and the oxidized dye molecules, and then reducing the charge recombination and the dark current. In a word, the direct consequence of the abovementioned structural advantages of the AMS microspheres is that the $J_{sc}$ and $V_{oc}$ of the Ti foil-based quasi-solid state DSSCs using AMS microspheres are higher than those of the device using P25 nanoparticles, and then causing a superior photovoltaic performance with a conversion efficiency of 7.16%, which was improved by 34% compared to the P25 film-based one (5.34%).

For further insight into the differences of interfacial charge transfer dynamics between AMS

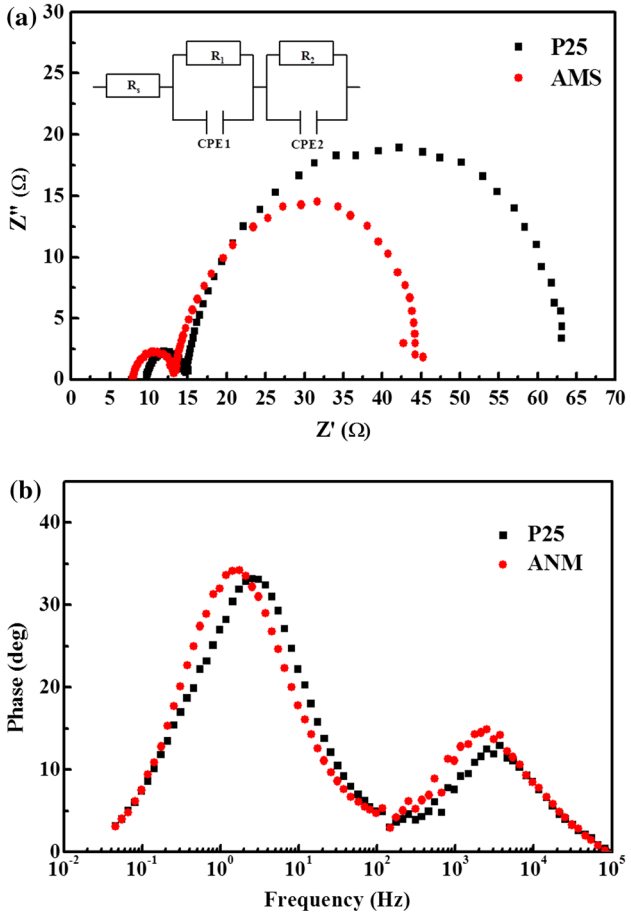


Fig. 7. Nyquist (a) and Bode (b) plots of the Ti foil-based quasi-solid state DSSCs fabricated with AMS or P25 film-based electrode under AM1.5G illumination.

microspheres and P25 nanoparticles film-based solar cells, electrochemical impedance spectra (EIS) were measured under back illumination of 100 mW cm$^{-2}$ light intensity. Figure 7 depicts the Nyquist and Bode plots of the fabricated two kinds of Ti-foil-based quasi-solid state DSSCs under illumination. According to the previous literature,[26,28–32] three semicircles usually can be observed from the Nyquist plot when a solar cell is controlled at an open-circuit condition under light illumination. The high-frequency semicircle (in kHz region) reflects the charge transfer resistance at the redox couple/counter electrode interface; the middle-frequency semicircle (in 10–100 Hz region) is attributed to the electron transport across the $TiO_2$ layer and their recapture by $I_3^-$ ions, and the low-

frequency semicircle (in the mHz region) is mainly relative to the Nernst diffusion of $I_3^-$ ions in the electrolyte.[27–29,31]

The Nyquist plots shown in Fig. 7a display only two main semicircles, which can be ascribed to the relatively high conductivity of the present iodine-free IL gel electrolyte.[30] It can cause the featureless semicircle attributed to the Nernst diffusion of $I_3^-$ ions in electrolyte.[30,33] Therefore, the photoelectrochemical parameters of those solar cells can be simulated using the simple equivalent circuit model inserted in Fig. 7a, and the relative fitted parameters are listed in Table II, where the series impedance $R_s$ is mainly related to the electrical resistance between the base resistance and the Ti foil/$TiO_2$ interface; $R_{ct1}$ represents the impedance associated with the charge transfer between the counter electrode and the electrolyte; and $R_{ct2}$ relates to the resistance of the electron accumulation/transport within the $TiO_2$ film and the charge transfer across the $TiO_2$/dye/electrolyte interfaces.[28,29]

As shown in Fig. 7a, the AMS film-based device displays an obviously smaller semicircle at the middle-frequency region with shift to lower frequency (ref. Bode plots in Fig. 7b) compared to the P25 film-based one. Because the semicircle at the middle-frequency region relates to the electron transport across the $TiO_2$ layer, it can be concluded that the electron transport resistance in the AMS film is smaller than that of the P25 film.[27] This is confirmed by $R_{ct2}$ values shown in Table II, whereby the AMS film-based device gives a 32.52 Ω $cm^2$ of $R_{ct2}$, much lower than that (48.71 Ω $cm^2$) of the P25 film-based one. Generally, it considered that a lower $R_{ct2}$ value indicates better $TiO_2$ nanoparticle interconnection, which is conducive to the electron transport across the $TiO_2$ layer.[28] Due to the one-dimensional nanotubes accumulated and wound in the AMS microspheres, the grain boundaries decrease significantly compared to P25 nanoparticles. Namely, the fibrous nanotubes in AMS microspheres are beneficial for the electron transport in the $TiO_2$ film, and then causing the reduced charge recombination and dark current.[26,29]

On the other hand, the iodine-free IL gel electrolyte used in the present devices has high viscosity,[30] which is not conducive to the penetration of the electrolyte in the $TiO_2$ film, and thus might result in the increase of the electron transport resistance at the electrolyte/$TiO_2$ interface, thereby increasing the $R_{ct2}$ value. However, the unique three-dimensional network-like porous micro/nanostructures of the AMS microspheres could provide a much larger surface area and pore volume compared to the P25 nanoparticles, and the larger diameter of the microspheres (5 $\mu$m) would contribute to the better penetration of the gel electrolyte in the $TiO_2$ porous film. Therefore, the AMS film-based solar cell shows much smaller $R_{ct2}$ value than the P25 film-based one. In addition, the $R_s$ value of the AMS film electrode is 7.97 Ω $cm^2$, also lower than the that (9.68 Ω $cm^2$) of the P25 film-based one (Table I), indicating that the AMS film-based device has lower internal resistance than the P25 film-based one. Both of them would be due to the fact that AMS microspheres have the three-dimensional network-like structure formed by the accumulation and winding of fibrous anatase $TiO_2$ nanotubes.

The electron lifetime ($\tau_n$) of DSSCs can be calculated using the formula $\tau_n = 1/(2\pi f)$, where $f$ is the frequency corresponding to the peak of the low-frequency region in the Bode plots.[26,29] In Bode plots shown in Fig. 7b, the characteristic frequency peaks of the AMS film-based device shifts to lower frequency, demonstrating a longer electron lifetime can be obtained.[32] The calculated electron lifetime of the AMS film-based device is 91.62 ms, much longer than that (62.4 ms) of the P25 film-based one fabricated under the same conditions. It indicates that the AMS film-based device has a lower charge recombination rate than the P25 film-based one, which then results in the AMS film-based device showing higher photocurrent density and lower dark current. This is consistent with the above $J$–$V$ (Fig. 5) and dark current (Fig. 6) curves.

The charge recombination processes in the quasi-solid state DSSCs fabricated with AMS microspheres and P25 nanoparticles film electrodes were investigated by using the open-circuit voltage decay (OCVD) curves. Figure 8 depicts the OCVD and the corresponding electron lifetime ($\tau'_n$)–$V_{oc}$ relation curves of the two kinds of Ti foil-based DSSCs. Under the used open-circuit and dark conditions, the electron transport impedance in the $TiO_2$ film does not affect the OCVD measurement because no current flow through the solar cells. As can be seen from Fig. 8a, the $V_{oc}$ decay trend of the AMS film-based solar cell in the dark state is slower than that of the P25 film-based one, which means that the AMS film-based device has a longer electron lifetime

**Table II. Photochemical parameters of the Ti foil-based quasi-solid state DSSCs fabricated with AMS or P25 film**

| Device | $R_s$ (Ω $cm^2$) | $R_{ct1}$ (Ω $cm^2$) | $R_{ct2}$ (Ω $cm^2$) | $f$ (Hz) | $\tau_n$ (ms) | CPE1 (F) | CPE2 (F) |
|---|---|---|---|---|---|---|---|
| P25 | 9.68 | 4.73 | 48.71 | 2.55 | 62.44 | $3.05 \times 10^{-5}$ | $4.26 \times 10^{-3}$ |
| AMS | 7.97 | 4.75 | 35.52 | 1.74 | 91.62 | $7.19 \times 10^{-5}$ | $7.31 \times 10^{-3}$ |

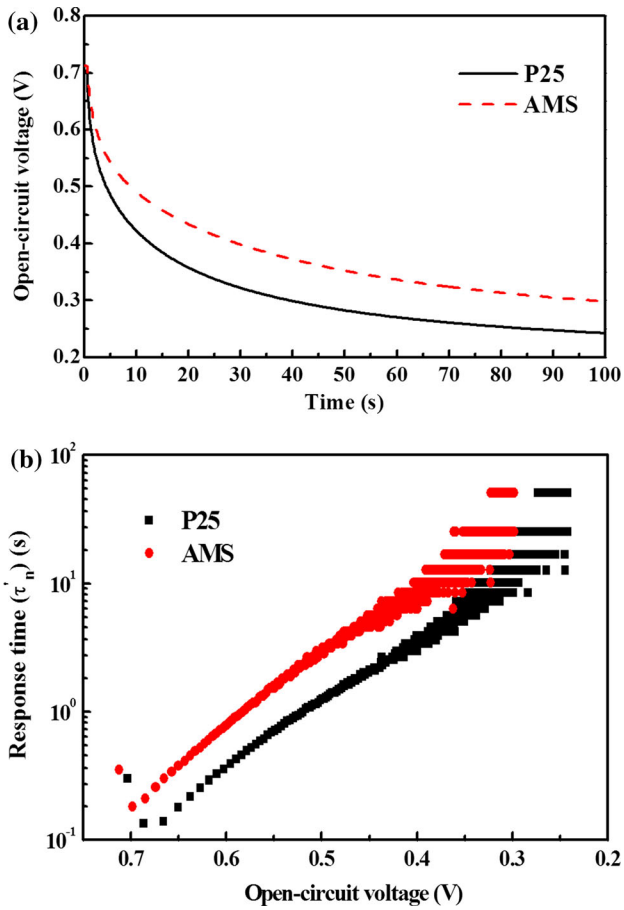


Fig. 8. OCVD (a) and $\tau'_n$–$V_{oc}$ (b) curves of the Ti foil-based quasi-solid state DSSCs fabricated with AMS or P25 film-based electrode.

and a lower charge recombination than the P25 film-based one.

Since the difference of cell's $V_{oc}$ can change the $\tau'_n$ values due to the Fermi level shift of $TiO_2$, the shape of $\tau'_n$–$V_{oc}$ relation curve of the solar cell can qualitatively reflect the effects of the electron traps on the recombination reaction. According to the previous literature,[34,35] the shape of the $\tau'_n$–$V_{oc}$ curve can be qualitatively divided into three regions such that the lifetime is dominated by different factors: an inverted parabola at a low-voltage region corresponding to the reciprocal of the acceptor electrolyte species density; an exponential dependence at a medium-voltage region due to the internal trapping and detrapping; and a constant lifetime at high voltage related to free electrons. Figure 8b gives the corresponding $\tau'_n$–$V_{oc}$ relation curves derived from the OCVD measurements based on Eq. 1,

$$\tau_n' = -\frac{k_B T}{e}\left(\frac{dV_{oc}}{dt}\right)^{-1}, \qquad (1)$$

where $k_B$ is the Boltzmann constant, $T$ is the temperature, and $e$ is the electron charge.[26]

As can be seen from Fig. 8b, the $\tau'_n$–$V_{oc}$ curve of the AMS film-based device locates above that of the P25 film-based one in the whole voltage region, indicating that the electron recombination in the AMS film is slower than that of the P25 film, which leads to the longer electron lifetime of the corresponding solar cell. It means that the AMS film can more efficiently transport the injected electrons and retard the charge recombination as compared to the P25 film. This is consistent with the results of the above $J$–$V$, dark current and EIS analyses.

The unique hierarchical micro/nano-structure of the present AMS microspheres leads to a much larger surface area and pore volume than that of the P25 nanoparticles, which not only increases the dye-loading amount, but also facilitates the penetration of the IL gel electrolytes in the $TiO_2$ porous film electrode, thereby enhancing the $J_{sc}$ value of the AMS film-based solar cell. In addition, the one-dimensional $TiO_2$ nanotubes accumulated and wound in the AMS microspheres provides a direct path for the electron transport in the film electrode, which reduces the grain boundaries and surface electron traps in the $TiO_2$ porous film and promotes the electron transport. As a result of the above unique structural features, the $J_{sc}$ and $V_{oc}$ of the AMS film-based device are higher than those of the P25 film-based one, which then results in a conversion efficiency of 7.16%, improved by 34% when compared to the P25 film-based one (5.34%). Namely, the AMS hierarchical microspheres with three-dimensional network-like porous structure formed by the accumulation and winding of fibrous anatase $TiO_2$ nanotubes ensure high specific surface area and pore volume with better electron conductivity and low electron recombination, which can overcome the shortcomings of the traditional one-dimensional nanostructures and nanoparticle films that have smaller surface area and are not conducive to the penetration of the gel electrolyte. These results provide a new insight for more efficient Ti foil-based quasi-solid-state DSSCs by optimizing the composition and structure of the photoanode films.

## CONCLUSIONS

In summary, prepared fibrous anatase $TiO_2$ nanotubes-aggregated microspheres (AMS) with porous structure and high specific surface area not only provide sufficient interspaces for dye-loading and penetration of the gel electrolyte with high viscosity in the film electrode, but also provide a good path for electron transport and reduce the charge recombination within the film electrode, and, therefore, is superior to the conventional $TiO_2$ nanoparticles for application in DSSCs. As a result of the above unique structural features, the conversion efficiency of the AMS film-based solar cell was 7.16%, which was improved by 34%, compared to the P25 film-based one (5.34%). The results presented here

provide a different insight for more efficient Ti foil-based DSSCs by optimizing the composition and structure of the photoanode films.

## ACKNOWLEDGMENTS

This work was supported by the state project of D.P.R. Korea 'Development of the Perovskite Solar Cell' (No. 2016-05).

## REFERENCES

1. B. O'Regan and M. Grätzel, *Nature* 353, 737 (1991).
2. S. Mathew, A. Yella, P. Gao, R. Humphry-Baker, B.F.E. Curchod, N. Ashari-Astani, I. Tavernelli, U. Rothlisberger, M.K. Nazeeruddin, and M. Grätzel, *Nat. Chem.* 6, 242 (2014).
3. J.M. Kroon, N.J. Bakker, H.J.P. Smit, P. Liska, K.R. Thampi, P. Wang, S.M. Zakeeruddin, M. Grätzel, A. Hinsch, S. Hore, U. Wurfel, R. Sastrawan, J.R. Durrant, E. Palomares, H. Pettersson, T. Gruszecki, J. Walter, K. Skupien, and G.E. Tulloch, *Progr. Photovolt. Res. Appl.* 15, 1 (2007).
4. S.G. Hashmi, M. Özkan, J. Halme, S.M. Zakeeruddin, J. Paltakari, M. Grätzel, and P.D. Lund, *Energy Environ. Sci.* 9, 2453 (2016).
5. K. Fan, R.J. Li, J.N. Chen, W.Y. Shi, and T.Y. Peng, *Sci. Adv. Mater.* 5, 1596 (2013).
6. J.L. Xu, S.F. Wu, J.P. Jin, and T.Y. Peng, *Nanoscale* 8, 18771 (2016).
7. J.L. Xu, S.F. Wu, J.H. Ri, J.P. Jin, and T.Y. Peng, *J. Power Sources* 327, 77 (2016).
8. J. Wang and Z.Q. Lin, *J. Phys. Chem. C* 113, 4026 (2009).
9. J. Wei, J. Yao, X. Zhang, W. Zhu, H. Wang, and M. Rhodes, *Mater. Lett.* 61, 4610 (2007).
10. H.C. He, C.B. Zhang, T. Liu, Y.H. Cao, N. Wang, and Z.H. Guo, *J. Mater. Chem. A* 4, 9362 (2016).
11. H.L. Jia, M.D. Zhang, W. Yan, X.H. Ju, and H.G. Zheng, *J. Mater. Chem. A* 4, 11782 (2016).
12. M. Ye, X. Xin, C. Lin, and Z. Lin, *Nano Lett.* 11, 3214 (2011).
13. J. Lin, Y.U. Heo, A. Nattestad, Z. Sun, L. Wang, J.H. Kim, and S. Dou, *Sci. Rep.* 4, 5769 (2014).
14. A.K. Sinha, S. Jana, S. Pande, S. Sarkar, M. Pradhan, M. Basu, S. Saha, A. Pal, and T. Pal, *CrystEngComm* 11, 1210 (2009).
15. N.P. Thuy-Duong, E.J. Kim, S.H. Hahn, W.J. Kim, and E.W. Shin, *J. Colloid Interface Sci.* 356, 138 (2011).
16. M.D. Ye, D.J. Zheng, M.Y. Wang, C. Chen, W.M. Liao, C.J. Lin, and Z.Q. Lin, *ACS Appl. Mater. Interfaces* 6, 2893 (2014).
17. J.G. Yu, J.J. Fan, and K.L. Lv, *Nanoscale* 2, 2144 (2010).
18. B. Liu and E.S. Aydil, *J. Am. Chem. Soc.* 131, 3985 (2009).
19. X.F. Yang, C.J. Jin, C.L. Liang, D.H. Chen, M.M. Wu, and J.C. Yu, *Chem. Commun.* 47, 1184 (2011).
20. J. Wang, L. Zhao, V.S.Y. Lin, and Z.Q. Lin, *J. Mater. Chem.* 19, 3682 (2009).
21. X.J. Feng, K. Shankar, O.K. Varghese, M. Paulose, T.J. Latempa, and C.A. Grimes, *Nano Lett.* 8, 3781 (2008).
22. J. Wang and Z.Q. Lin, *Chem. Mater.* 20, 1257 (2008).
23. M.M. Yahkostupov, M. Zamkov, and F.N. Castellano, *Energy Environ. Sci.* 4, 998 (2011).
24. P. Roy, S. Berger, and P. Schmuki, *Angew. Chem. Int. Ed.* 50, 2904 (2011).
25. P. Schmuki, J.M. Macak, M. Zlamal, and J. Krysa, *Small* 3, 300 (2007).
26. W.W. Liu, H.G. Wang, X.F. Wang, M. Zhang, and M. Guo, *J. Mater. Chem. C* 4, 11118 (2016).
27. K. Fan, J.N. Chen, F. Yang, and T.Y. Peng, *J. Mater. Chem.* 22, 4681 (2012).
28. K. Fan, T.Y. Peng, J.N. Chen, X.H. Zhang, and R.J. Li, *J. Power Sources* 222, 38 (2013).
29. T.Y. Peng, W.Y. Shi, S.F. Wu, Z.H. Ying, and J.H. Ri, *Mater. Chem. Phys.* 164, 238 (2015).
30. J.H. Ri, J.P. Jin, J.L. Xu, T.Y. Peng, and K.I. Ryu, *Electrochim. Acta* 201, 251 (2016).
31. F. Sauvage, F. Di Fonzo, A. Li Bassi, C.S. Casari, V. Russo, G. Divitini, C. Ducati, C.E. Bottani, P. Comte, and M. Grätzel, *Nano Lett.* 10, 2562 (2010).
32. R. Kern, R. Sastrawan, J. Ferber, R. Stangl, and J. Luther, *Electrochim. Acta* 47, 4213 (2002).
33. K. Fan, T.Y. Peng, J.N. Chen, and K. Dai, *J. Power Sources* 196, 2939 (2011).
34. A. Zaban, M. Greenshtein, and J. Bisquert, *ChemPhysChem* 4, 859 (2003).
35. J. Bisquert, A. Zaban, M. Greenshtein, and I. Mora-Sero, *J. Am. Chem. Soc.* 126, 13550 (2004).